Cold Regions Research and Engineering Laboratory

US Army Corps of Engineers®
Engineer Research and Development Center

Propagation of Uncertainties in Sea Ice Thickness Calculations from Basin-Scale Operational Observations

A Report Prepared for the International Ice Charting Working Group and the National/Naval Ice Center

Cathleen A. Geiger   September 2006

Cover Photo: Sea-ice ridge split by a fracture event in the Beaufort Sea during the Sea-Ice Mechanics Initiative (SIMI) experiment in March 1994. The fracture has laterally opened to form a lead that was in the process of refreezing when this photograph was taken (photograph by Bruce Elder).

Propagation of Uncertainties in Sea Ice Thickness Calculations from Basin-Scale Operational Observations

A Report Prepared for the International Ice Charting Working Group and the National/Naval Ice Center

Cathleen A. Geiger

Cold Regions Research and Engineering Laboratory
U.S. Army Engineer Research and Development Center
72 Lyme Road
Hanover, NH03755

Final report

Abstract: Sea ice serves as a natural flux monitor of the global heat balance. This capability is attributed to the unique location of sea ice at the interface of the world's two largest circulation systems—the air and ocean. The increased awareness of warming in the polar region has precipitated increased efforts to measure sea ice thickness as an index for global heat changes. This increased awareness has brought with it the development of several new prototype in situ, telemetry, and satellite remote sensing instruments. Each of these provides a means for measuring part or all of the frozen material at the air–sea interface, but each comes with considerable limitations. The integration of these measurements into basin-scale objective analysis fields will serve as important input for global climate models, much like current-day weather forecasting systems and the El-Niño monitoring system. As the various thickness monitoring tools begin to develop, it is critical that standards be established to record the quality of these data. This report addresses the data quality issues by examining a robust method for tracking uncertainties in measurements. The data sets considered are the two existing operational basin-scale systems: ship-based observations and satellite composite analysis. Illustrative examples are included.

Contents

Figures and Tables

Figures

Tables

Preface

1   INTRODUCTION

Sea ice is not uniform, level, or continuous. It is a mixture of different ice types, each of which responds differently to mechanical and thermal forcing. Numerous studies (e.g., Allison 1989; Worby et al. 1996, 1998) show that a high percentage of the Antarctic pack ice is composed of thin ice types and open water. The distribution of these different ice types is important in determining other characteristics of the pack, as shown in the Arctic by Thorndike et al. (1975), who concluded that the aggregate properties of the pack are determined from the properties and relative abundance of each constituent. It is, therefore, essential to know the distribution of ice thickness.

According to Wadhams (1996), there are four methods commonly used for measuring all or part of sea ice thickness: 1) upward-looking or side-scanning sonar, 2) air- and space-borne laser altimeters, 3) electromagnetic techniques in combination with lasers, and 4) drilling. Sonar methods are the most effective in measuring sub-surface draft, which constitutes the larger part of the total thickness distribution owing to the buoyancy of ice in water. Airborne laser profilometers called LIDAR (light detection and ranging) are the main source for sea ice freeboard heights. Electromagnetic techniques typically involve long, cylindrical, RADAR-range emitters in the 10–50 kHz range (Wadhams 1996), which respond to eddy currents at the base of the ice. These are effective when dragged across the ice, mounted from a ship, or suspended from a low-flying helicopter, but are still highly experimental, few in number, and very expensive. The fourth, drilling, is the most accurate. It is painfully slow but is the primary form of validation for all other techniques.

Regional empirical relationships between freeboard and draft, as described, for example, in Wadhams and Comiso (1992) and Allison and Worby (1994), can be used in combination with regional snow estimates to compute snow and total ice thickness from surface freeboard measurements. Because of such relationships, the long-term goal for sea ice thickness monitoring is a space-borne laser with basin-wide repeat coverage at regular intervals.

1.1 Operational Methods

Two methods within the operational community are currently used to in-directly estimate sea ice: ship-based observations and weekly ice charts derived from subjective analysis of satellite images. Both follow the World Meteorological Organization's (WMO) recommended 16 distinct ice thickness categories or stages-of-development (WMO 1970).

1.1.1 Weekly Ice Charts

From 1972 to the present, the National Ice Center (NIC) has been providing global sea ice analysis and forecasts to the U.S. military and civilian sectors. The most widely used products are the NIC weekly sea ice charts that span the entire Arctic, including the sub-Arctic and the Antarctic. Ice charting standards were formalized in 1970 under the World Meteorological Organization (WMO 1970) with the increased international interest in safe navigation in ice-covered waters. Although these standards have evolved over time with improved interpretive capabilities from remotely sensed data, the basic chart content has remained unchanged for more than 30 years (Dedrick et al. 2001). These NIC archived charts, which have a traditional operational nature, remain a significant, under-utilized scientific record of Northern and Southern Hemisphere sea ice conditions from 1972 to the present.

The NIC produces its charts using a multi-sensor, multi-source approach (Dedrick et al. 2001). Remote sensing is a powerful tool to monitor sea ice coverage. Many sensors can provide valuable information on sea ice, especially passive microwave instruments such as Scanning Multi-frequency Microwave Radiometer (SMMR) and Scanning Multi-frequency Microwave/Imager (SSM/I). NIC also incorporates visible and infrared imagery data to overcome some of the limitations of passive microwave data. As more advanced remote sensing technology has become available, such as synthetic aperture radar (SAR), since 1995, they have also been incorporated into the analysis process (Bertoia et al. 1998). In addition, analysts' expertise and data from meteorological and oceanographic models and data systems are utilized in creating the ice charts. The results of this integrative approach are composite pictures of ice conditions, including ice concentration, ice stage, and ice form. Dedrick et al. (2001) provides a detailed explanation of the analytical process used by NIC analysts.

1.1.2 Ship-Based Method

The ship observations are currently the only effective form of basin-scale in situ ice thickness measurements for the Antarctic owing to submarine restrictions and high incidences (50% rate) of berg hits on moorings (Strauss and Fahrbach 1998). Ship observations are organized under the international Antarctic Sea-ice Processes and Climate (ASPeCt) program of the international Scientific Committee on Antarctic Research (SCAR). The archive currently comprises more than 20,000 stations of sea ice type, thickness, compactness, topography, floe size, and snow cover (Worby and Ackley 2000) from national programs of the U.S., Australia, Russia, U.K., and Germany. In the Arctic, ship observations are currently not systematically recorded for either operational or scientific purposes because the current ice thickness (with large ridges) prevents straight-line ship tracks through sea ice as required in existing ASPeCt protocols. However, a modification of sampled stations spaced at least 6 nautical miles apart could be implemented for the Arctic if there were a mechanism for integrating ship-based observations from the Arctic with the currently active Antarctic ship observation system.

Worby et al. (1998) presented climatology of sea ice thickness data for east Antarctic between 60°S and 150°E based on ship data from the ASPeCt data archive. This climatology clearly shows the seasonal variability in Antarctic sea ice thickness distribution, with the modal thickness moving from the thinnest category in March to a maximum of 0.6–0.8 m in August and then back to the open water category in December, when the ice-covered area of the pack is only 40%. Hence, when carefully observed and quality controlled, these data provide a unique and highly valuable source of Antarctic sea ice thickness data. At the current rate of Arctic sea ice decay, the current Antarctic sea ice thickness variability may provide us with insight into a potential future Arctic sea ice state, which would allow measurement techniques specific to the Antarctic to be applied to the Arctic.

In the Antarctic, ASPeCt ship-based ice observations are made by visually partitioning the horizon into three categories of ice types, each of which is composed of relative amounts of level and deformed ice. The deformed ice is classified as ridges that can be vertically described as a composite of 1) level ice with, 2) an unseen keel below, and 3) a sail above. These ridges represent a certain percentage of the area covering a given thickness category. Once the observer has assessed the relative amounts of each ice type by area, the thickness of the level ice is recorded by looking down from the

bridge to the ship's side to view the upturned floes along the hull. This effort is made for each of the three ice categories. A reference buoy of known diameter is often used as a gauge to estimate thickness. Next, observers look to the horizon to estimate the percentage and heights of any ridges. The total ice thickness is calculated using an empirical relationship involving the area of each ice category, observed level ice, ridged height, and area of ridged ice. The equations for the ridged relationship (provided in Section 5.1) are based on drill data. Results of these observations are entered into a log and electronic spreadsheet including time, geographical information, and meteorological data. Table 1 and Section 6.1 will provide an example to walk through the details of this type of observation.

1.2 Problem Statement

Given the collection of data types above, a critical question to ask is: how does one combine results from these data types to provide a quantitative data set that can be used for basin-scale applications? The first step in this process is to provide a systematic means for quantifying the uncertainty in each data set. Once that is determined, a weight can be assigned to quantify the data quality, for example, in data assimilation or objective analysis mapping. This first step is the goal of this report.

Essentially, given a collection of measurements and associated errors, one needs to determine the propagation of errors through a series of mathematical computations, including sums and differences, products and quotients, and statistical averages. This report reviews the framework needed. First, the basic rules of error propagation are described based on general rules from mathematics and physics. Next, the statistical principles relevant to error propagation are reviewed. Finally, a demonstration of these principles is provided in the context of the above discussion using actual data from the NIC and ship-based methods.

2   BASIC RULES OF ERROR PROPAGATION

Error propagation is based on multivariate differential principles whereby a function (F) with known uncertainties of size (dx, dy, ...) can be expressed as

$$dF = \frac{\partial F}{\partial x} dx + \frac{\partial F}{\partial y} dy + \cdots \qquad (1)$$

Considering the changes to be finite (i.e., $dx \approx \Delta x$), one sees that the variance of these changes ($s_x^2 = \overline{(\Delta x)^2}$) propagate such that the variance of the function $(dF)^2 \approx \overline{(\Delta F)^2} = s^2$ becomes

$$\overline{(\Delta F)^2} = \left(\frac{\partial F}{\partial x}\right)^2 \overline{(\Delta x)^2} + \left(\frac{\partial F}{\partial y}\right)^2 \overline{(\Delta y)^2} + \cdots + \left[2\frac{\partial F}{\partial x}\frac{\partial F}{\partial y}\overline{\Delta x \Delta y}\right] + \cdots \qquad (2)$$

where the bar denotes the average of the squared changes and the cross-terms are defined as the *covariance*. The equation above is equivalent to

$$s^2 = \left(\frac{\partial F}{\partial x}\right)^2 s_x^2 + \left(\frac{\partial F}{\partial y}\right)^2 s_y^2 + \cdots + (\text{covariances}). \qquad (3)$$

If all the measured quantities are independent of each other (i.e., orthogonal), then the covariance vanishes.

All the basic rules of error propagation are rendered from the above relationship. The first of these rules regards the sum or difference of measured values (x, y, z) with constant coefficients (a, b, c) such that $F = ax + by + cz$. From the basic formulation above, the variance of this function is

$$\overline{(dF)^2} \approx s^2 = a^2 s_x^2 + b^2 s_y^2 + c^2 s_z^2 + \text{covariance} \qquad (4)$$

where terms like s_x^2 denote the individual variance or uncertainties of each of the measured values. In words, this means that uncertainties of terms with like units combine in quadrature.

Likewise for products or quotients, such as $F = axyz$

$$\overline{(dF)^2} \approx s^2 = \left[\left(\frac{s_x}{x} \right)^2 + \left(\frac{s_y}{y} \right)^2 + \left(\frac{s_z}{z} \right)^2 \right] F^2 \qquad (5)$$

which comes about by noting that $\dfrac{\partial F}{\partial x} = ayz$,

which can be multiplied by $1 = x/x$ such that $\left(\dfrac{\partial F}{\partial x} \right)^2 = \left(\dfrac{F}{x} \right)^2$.

In words, what is happening is that the absolute errors are first converted to relative errors having dimensionless units and then added in quadrature to obtain the relative error of the function F. To convert back to the absolute error (i.e., with units), the relative error is then multiplied by the function F.

3   GENERAL APPLICATIONS

The basic rules follow those on web site:
http://instructor.physics.lsa.umich.edu/ip-labs/tutorials/errors/prop.html

*   Rule 1: When adding or subtracting two values x and y, the absolute
    uncertainty of $x + y$ or $x - y$ is found by adding the absolute uncertain-
    ties δx and δy in quadrature. This essentially means that you add the
    variances (variance being the square of the standard deviation or un-
    certainty at one sigma level based on a normal distribution). You then
    take the square root of the summed variances to get back to the propa-
    gated standard deviation or plus-minus uncertainty value. This is writ-
    ten as

$$\delta(x - y) = \delta(x + y) = [(\delta x)^2 + (\delta y)^2]^{1/2}. \tag{6}$$

*   Rule 2: When multiplying or dividing x and y, the fractional uncer-
    tainty of x times y or x/y is obtained by adding the relative uncertain-
    ties $\delta x/x$ and $\delta y/y$ in quadrature as

$$\delta(x\,y)/(x\,y) = \delta(x/y)/(x/y) = [(\delta x/x)^2 + (\delta y/y)^2]^{1/2}. \tag{7}$$

*   Rule 3: The fractional uncertainty on x to a power n is n times the frac-
    tional uncertainty of x or

$$\delta(x^n)/(x^n) = n(\delta x/x). \tag{8}$$

*   Rule 4: The absolute uncertainty on an arbitrary function of x is found
    by taking the derivative of that function, evaluating it at the measure-
    ment x_0, taking the absolute value, and multiplying the result by the
    absolute uncertainty of x. Mathematically this is,

$$\delta F(x_0) = |\, dF/dx\,|_{x=x_0}\ \delta x_0. \tag{9}$$

Angular measurements must be expressed in radians. Rule 4 is the most
general application and ties in closely with that presented in Section 2.

4   RELATED STATISTICS

According to Kish (1965) and Stark (2002), any observation can be characterized as the sum of the following

$$\text{estimator} = \text{parameter} + \text{bias} + \text{chance variability} \tag{10}$$

where estimator is an estimate of a sample taken from some population, parameter is a property of the population (i.e., the truth), bias is a systematic difference between some measurement and the truth, and chance variability is the random sampling error, which has a long-term mean of zero from the truth such that $E(\text{chance variability}) = 0$, where $E(\ )$ is the operator denoting an estimate of the term in parenthesis (read as "estimate of"). It is also sometimes referred to as the "expectation of," depending on which text one refers.

The variance (s^2) is a measure describing the range of the sampling error (i.e., average of the spread of the estimate) and can be expressed in two different forms (Stark 2002), namely,

$$s^2 = E([\text{estimator} - E(\text{estimator})]^2) \tag{11}$$

$$= E([\text{chance variability}]^2). \tag{12}$$

The variance is also often referred to using the operator notation $V(\ )$, which stands for "variance of." Note, while $E(\text{chance variability}) = 0$, it is clear from eq 12 that $E[\ (\text{chance variability})^2\ ] \neq 0$. This relationship provides the means for quantifying the variability as the expectation of the chance variability squared. Furthermore, the overall mean-squared-error (*MSE*) is

$$MSE = s^2 + \text{bias}^2 \tag{13}$$

which includes errors associated with any bias and, hence, relative to eq 10, implies that $E(\text{estimator}) = \text{parameter} + \text{bias}$ (Stark 2002). As additional nomenclature, the standard error (*SE*) is also called the standard deviation, which is the square-root of the variance ($SE = s = \sqrt{s^2}$).

To relate this statistical notation to that demonstrated in Section 3, reconsider the equation $F = ax + by + cz$. Using the statistical operators for estimate $E(\ )$ and variance $V(\ )$, one computes $E(F)$ (read as the "estimated value for F") as (Hines and Montgomery 1990)

$$E(F) = E(ax + by + cz) \tag{14}$$

$$= E(ax) + E(by) + E(cz) \tag{15}$$

$$= aE(x) + bE(y) + cE(z) \tag{16}$$

and $V(F)$ (read as the "variance of F") as (Hines and Montgomery 1990)

$$V(F) = E(F - E(F))^2 \tag{17}$$

$$= a^2 V(x) + b^2 V(y) + c^2 V(z) + \text{covariances.} \tag{18}$$

If one substitutes terms like $E(x)$ with x and $V(x)$ with s_x^2, these equations take on the same form as those for rules of error propagation (e.g., eq 4). The generalized form is

$$Y = w_0 + \sum_{i=1}^{n} w_i X_i \tag{19}$$

$$E(Y) = w_0 + \sum_{i=1}^{n} w_i E(X_i) \tag{20}$$

$$V(Y) = \sum_{i=1}^{n} w_i^2 V(X_i) + \sum_{i=1}^{n}\sum_{j=1}^{n} (1 - \delta_{ij}) w_i w_j Cov(X_i, X_j) \tag{21}$$

where the coefficients (w_i) are weight functions, $Cov(\ )$ denotes the covariance operator, and Δ is the Kronecker delta equal to 1 when $i = j$ and zero when $i \neq j$ (i.e., $1 - \Delta_{ij}$ is used for computing the covariance for all cases where $i \neq j$).

If one applies these rules to a statistical mean of independent measurements (i.e., $Cov(X_i, X_j) = 0$) for which the coefficients (w_i) represent an arbitrary fraction of the total number of points (n), then

$$\bar{x} = \sum_{i=1}^{p} w_i x_i \tag{22}$$

where $n = \sum_{i=1}^{p} 1/w_i$ for the case $p = n$, $w_i = 1/n$, and this reduces to the well known simple statistical mean

$$\bar{x} = \frac{1}{n}\sum_{i=1}^{n} x_i. \tag{23}$$

The corresponding sample variance ($V(Y) = s^2$) can be written in two forms (Hines and Montgomery 1990):

$$V(Y) = s^2 = \sum_{i=1}^{p} w_i^2 V(X_i) = \sum_{i=1}^{p} w_i^2 s_i^2 \tag{24}$$

$$s^2 = \frac{n}{n-1}\left[\sum_{i=1}^{p} w_i x_i^2 - (\sum_{i=1}^{p} w_i x_i)^2\right] \tag{25}$$

and for the case $p = n$, $w_i = 1/n$, one arrives at the simple forms

$$s^2 = \frac{1}{n^2}\sum_{i=1}^{n} s_i^2 \tag{26}$$

$$s^2 = \frac{1}{n-1}\left[\sum_{i=1}^{n} x_i^2 - (\sum_{i=1}^{n} x_i)^2/n\right] \tag{27}$$

$$= \frac{1}{n-1}\sum_{i=1}^{n}(x_i - \bar{x})^2 \tag{28}$$

Note from eq 24 that the standard deviation is expressed as

$$s = \sqrt{\sum_{i=1}^{p} w_i^2 s_i^2} \tag{29}$$

which will be applied often in the upcoming applications.

5   APPLICATIONS

5.1 Ship-Based Sea Ice Thickness

The average ice thickness (cm) from a ship observation is defined as

$$\overline{z}_n(\lambda, \phi, t) = \hat{\overline{z}}_n \pm \overline{z}'_n \tag{30}$$

for $n = 1,...,N$ observations at locations of specified longitude (λ), latitude (Φ), and time (t). The $\hat{}$ is used throughout to indicate an estimated value while $'$ (i.e., prime) is used to indicate uncertainty. The estimated average ice thickness at each observation is defined as (eq 22)

$$\hat{\overline{z}}_n = \sum_{i=1}^{I} \hat{c}_i \hat{z}_i \tag{31}$$

for $i = 1,...,I$ ice categories, which may include the three standard ice categories plus up to three ridged ice categories. The open water fraction is automatically incorporated using this method or can be computed directly with a thickness of zero.[*] Note that in this case the ice concentration value is serving as a weight function when tallying the contributions from each thickness category.

Using the standard rules of error propagation (eq 4 and 5), one can define the uncertainty as

$$\overline{z}'_n = \left[\sum_{i=1}^{3} \left\{ \left(\left(\frac{c'_i}{\hat{c}_i} \right)^2 + \left(\frac{z'_i}{\hat{z}_i} \right)^2 \right) (\hat{c}_i \hat{z}_i)^2 \right\} \right]^{1/2}. \tag{32}$$

In eq 32, the observed quantity of ice thickness for each of the three ice categories is computed via

$$z_i = \hat{z}_i \pm z'_i; \tag{33}$$

---

[*] There remains the unresolved issue of how to include open water fraction versus zero ice thickness into probability distributions of ice thickness. The ship observation records make this distinction when the thinnest ice category has a thickness of zero distinct from the open water fraction. However, the average ice thickness is based on a chosen geographical area including the open water fraction.

while the area of each of these ice categories is described by a partial concentration (percent of total visible area) computed as

$$c_i = \hat{c}_i \pm c_i'$$ (34)

such that the sum of all three partial concentrations equals the total ice concentration.

The estimated ice thickness at each ice category is computed as

$$\hat{z}_i = \hat{z}_u + \hat{z}_r + \hat{z}_s$$ (35)

where $\hat{z}_u$, $\hat{z}_r$, and $\hat{z}_s$ represent level ice, ridged ice, and snow, respectively, with the ridged ice thickness estimated using the empirical formulation

$$\hat{z}_r = 2.7S + \hat{z}_u$$ (36)

such that S is the sail height of the ridge. Assuming a triangular shape for a ridge, one finds that the area of a ridge is equal to $AR/2$, where A is the area of the thickness category and R is the percentage of that thickness category covered by ridges. This product is divided by 2 because of the triangular shape of a ridge. To conserve both the mass and the height, the area of level ice is computed as $A'=A(1 - R/2)$. This area estimate is used to partition the thickness into two weighted statistical bins: a level height and ridged height.

Judiciously chosen initial uncertainties based on the ASPeCt archive are

$$c_i' = 10\%$$ (37)

$$z_u' = \begin{cases} 50\% & ;\ 0 \leq z < 10\,\text{cm} \\ 30\% & ;10 \leq z < 30\,\text{cm} \\ 20\% & \quad ;30\,\text{cm} \leq z \end{cases}$$ (38)

$$z_r' = 50\%$$ (39)

$$z_s' = 50\%$$ (40)

Average ice thickness within a selected region of longitude range ($\Delta\lambda$) and latitude range ($\Delta\Phi$) over selected time window of size Δt is expressed as

$$\tilde{z}_{\lambda\phi t} = \hat{\tilde{z}}_{\lambda\phi t} \pm \tilde{z}'_{\lambda\phi t} \tag{41}$$

where $\lambda = 1,...,L$ longitudes of width $\Delta\lambda$, $\Phi = 1,...,P$ latitudes of width $\Delta\Phi$, and $t = 1,...,T$ times of width Δt. If one now defines j as a subset of indices of n within a given $\lambda\,\Phi\,t$ bin for $j = 1,...,J$, then the mean and associated uncertainty, respectively (eq 23 and 26), are

$$\hat{\tilde{z}}_{\lambda\phi t} = \frac{1}{J}\sum_{j}\hat{\tilde{z}}_j(\lambda,\phi,t) \tag{42}$$

$$\tilde{z}'_{\lambda\phi t} = \frac{1}{J}\left[\sum_{j}\left(\overline{z}'_j(\lambda,\phi,t)\right)^2\right]^{1/2}. \tag{43}$$

Note that the weight for each station is assumed to be the same, producing the constant $1/J$. One modification to consider is the case where stations should be weighted because of visibility (or other weather related situations) or observer bias. If such is the case, the scheme described below for temporal averaging should be used instead.

The temporal mean ice thickness over select geographic regions $\Delta\lambda$, $\Delta\Phi$, and select parts of a year $\Delta\tau$ (e.g., weekly, monthly, seasonally; same size as Δt) is given by

$$\overline{\zeta}_{\lambda\phi\tau} = \hat{\overline{\zeta}}_{\lambda\phi\tau} \pm \overline{\zeta}'_{\lambda\phi\tau}. \tag{44}$$

If one defines k as the subset of indices of t within select λ, Φ indices and also at annual subdivisions of $\Delta\tau$ for $k = 1,...,K$ such that $k = k_{\lambda\Phi\tau}$, one gets estimates and associated uncertainty, respectively, of

$$\hat{\overline{\zeta}}_{\lambda\phi\tau} = \sum_{k}\left(\hat{\tilde{z}}_{\lambda\phi k}\, w_{\lambda\phi k}\right) \tag{45}$$

$$\overline{\zeta}'_{\lambda\phi\tau} = \left[\sum_{k}\left(\tilde{z}'_{\lambda\phi k}\, w_{\lambda\phi k}\right)^2\right]^{1/2}. \tag{46}$$

Note that a weighting is included to distinguish the number of samples contributing to each of the averages as per eq 24. The weight function $w_{\lambda\Phi k}$ equals

$$w_{\lambda\phi k} = \frac{J_{\lambda\phi k}}{\sum_i J_{\lambda\phi i}} \tag{47}$$

where $J_{\lambda\Phi k} = J$ in eq 43. A single station from a ship observation represents a specific area separated by at least 6 nautical miles with visual range to the horizon taken from the bridge of a ship. Conversely, a temporal average includes collections of stations at different times, where the number of stations at one time does not necessarily equal the number of stations at another time. It is for this reason that a weight is necessary as the number of stations at each time influences the average. As discussed above, this same weighting should be introduced for station averaging once protocols exist to characterize station bias introduced attributable to weather or observer effects.

Finally, ice thickness anomaly is defined as

$$\tilde{\zeta}_{\lambda\phi t} = \hat{\tilde{\zeta}}_{\lambda\phi t} \pm \tilde{\zeta}'_{\lambda\phi t} \tag{48}$$

where

$$\hat{\tilde{\zeta}}_{\lambda\phi t} = \hat{\tilde{z}}_{\lambda\phi t} - \hat{\tilde{\zeta}}_{\lambda\phi\tau} \tag{49}$$

$$\tilde{\zeta}'_{\lambda\phi t} = \frac{1}{J_{\lambda\phi t} + K_{\lambda\phi\tau}} \left[\left(\tilde{z}'_{\lambda\phi t} J_{\lambda\phi t} \right)^2 + \left(\overline{\zeta}'_{\lambda\phi\tau} K_{\lambda\phi\tau} \right)^2 \right]^{1/2} \tag{50}$$

for t equal to all sequential times and τ equal to all annual subdivisions such that

$$\frac{J_{\lambda\phi t}}{J_{\lambda\phi t} + K_{\lambda\phi\tau}} \quad \text{and} \quad \frac{K_{\lambda\phi\tau}}{J_{\lambda\phi t} + K_{\lambda\phi\tau}} \tag{51}$$

serve as weight functions propagated from eq 43 and 46. Note here that the $\tilde{z}$ terms are station averages over space while $\tilde{\zeta}$ denotes the average over time.

5.2 NIC Chart Estimates

The goal is to use the NIC charts to determine sea ice area, thickness, and mass on a climatological scale. The sea ice thickness can be computed using eq 31 and 32 described in the previous section and as demonstrated in Section 6. The ice charts are made up of polygons (also interpreted as outlined boundaries or aggregates) that are believed to contain common sea-ice properties. The sea ice extent is determined by the area of each polygon $\hat{a}$ that is subjectively drawn on the ice charts based on numerous remote sensing data and other input as described in the introduction. This extent calculation is accomplished by importing the sea ice chart information into Geographic Information System (GIS) software with the total extent for any given region of the chart defined as

$$\hat{A} = \sum_{p=1}^{P} \hat{a}_p \qquad (52)$$

for $p = 1,...,P$ polygons.

The boundaries of the ice chart polygons are believed to be accurate to within 20 km (Enomoto and Ohmura 1990). Using the BUFFER algorithm in ArcGIS 8.1, one can radially increase or decrease the perimeter contour around any polygon by a prescribed uncertainty distance and then recalculate the resultant area. Assuming an uncertainty of ±10 km based on Enomoto and Ohmura (1990), one first computes the area of a given polygon $\hat{a}_p$ using ArcGIS. Next, one increases the perimeter by 10 km radially and recomputes that new area $\hat{b}_p$ where the $\hat{b}$ stands for an estimate of the "buffered area" of each p polygon. The difference between these two areas is the upper bound absolute uncertainty and similarly for a lower bound. The relative uncertainty (or relative error) associated with this is

$$\tilde{a}'_p = \frac{\hat{b}_p - \hat{a}_p}{\hat{a}_p} \qquad (53)$$

Using the standard rules of error propagation, one defines the absolute uncertainty of the total error for each week as

$$A' = \left[\sum_{p=1}^{P} (\hat{b}_p - \hat{a}_p)^2 \right]^{1/2} \qquad (54)$$

for $p = 1,...,P$ polygons.

An estimate of the sea ice mass for each polygon in the Ross Sea is determined using

$$\hat{m}_p = \hat{\rho}\hat{a}_p\hat{\bar{z}}_p \tag{55}$$

where the sea ice density is currently approximated as the value $\rho = \hat{\rho} \pm \rho'$ = 920±10 kg m⁻³. The thickness $\hat{\bar{z}}_p$ is an average derived from the partial concentrations and, therefore, represents how much ice is present if all three ice types are combined and redistributed evenly across the area $\hat{a}_p$. The absolute uncertainty of the mass for each polygon is

$$m'_p = \left[\left(\left(\frac{\rho'}{\hat{\rho}}\right)^2 + \left(\tilde{a}'_p\right)^2 + \left(\frac{\bar{z}'_p}{\hat{\bar{z}}_p}\right)^2\right)\hat{m}_p^2\right]^{1/2} \tag{56}$$

The total regional sea ice mass follows as

$$M = \hat{M} \pm M' \tag{57}$$

$$\hat{M} = \sum_{p=1}^{P}\hat{m}_p \tag{58}$$

$$M' = \left[\sum_{p=1}^{P}(m'_p)^2\right]^{1/2} \tag{59}$$

for $p=1,...,P$ polygons for each weekly NIC chart.

To determine the average sea ice mass over several weeks, one indexes the weekly sea ice mass such that eq 57 is redefined to $M_k = \hat{M}_k \pm M'_k$ and then average using

$$\bar{M} = \hat{\bar{M}} \pm \bar{M}' \tag{60}$$

$$\hat{\bar{M}} = \frac{1}{K}\sum_{k=1}^{K}\hat{M}_k \tag{61}$$

$$\bar{M}' = \frac{1}{K}\left[\sum_{k=1}^{K}(M'_k)^2\right]^{1/2}$$ (62)

where one gives equal weighting to each of the $k = 1,...,K$ time periods.

5.3 Combined NIC Chart and Ship Measurements

Potentially, the most accurate estimate of sea ice mass balance will come from a combination of area measurements from NIC charts and thickness measurements from elsewhere (e.g., ship observations). This can be accomplished by

$$\hat{\tilde{z}}_p = \frac{1}{J_p}\sum_j \hat{\tilde{z}}_j$$ (63)

$$\tilde{z}'_p = \frac{1}{J_p}\left[\sum_j(\bar{z}'_j)^2\right]^{1/2}$$ (64)

where $j = 1,...,J$ is the subset of ship points contained in polygon p of the NIC charts.

This substitution changes the mass balance in eq 55 and 56 to

$$\hat{m}_p = \hat{\rho}\hat{a}_p\hat{\tilde{z}}_p$$ (65)

$$m'_p = \left[\left(\left(\frac{\rho'}{\hat{\rho}}\right)^2 + \left(\tilde{a}'_p\right)^2 + \left(\frac{\tilde{z}'_p}{\hat{\tilde{z}}_p}\right)^2\right)\hat{m}_p^2\right]^{1/2}$$ (66)

where the thickness term is now an estimate based on ship observations (denoted by the tilde over the z term instead of the bar over the z term) or some weighted result between ship, NIC charts, and other thickness sources.

6   EXAMPLE RESULTS

6.1 Ship-Based Examples

In this section, the step-by-step implementation of error propagation is examined using examples from ship observation records. Below in Table 1 is a sample ship station. Table 2 is a reconfiguration of Table 1 values into thickness categories. In principle, up to seven ice categories can be created from the information in Table 1, including the open water fraction, three level ice categories, and up to three deformed ice categories. In this example, the thinnest ice consists of only level ice while the medium and thick categories each have vertical protrusions in addition to the level ice field and, therefore, two sub-categories each (a level and deformed sub-category).

Table 1. Sample ship station. Data from ship observation taken at 65.62°S and 147.83°E on 27 April 1993 at 21:00.

	Sea Ice Category		
Property	Thick	Medium	Thin
Concentration (tenths)	3	6	1
Thickness (cm)	250	55	5
Ridging (tenths of category)	1	4	0
Sail Height (cm)	100	50	0
Snow Cover (cm)	150	20	0

Table 2. Statistical results (excluding snow) from ship observation taken at 65.62°S and 147.83°E on 27 April 1993 at 21:00.

Thickness		Concentration	
Value [cm]	Uncertainty [%]	Value [%]	Uncertainty [%]
Open Water	0	0	0
5	50	10.0	10
55	20	46.5	10
250	20	27.75	10
320	50	13.5	10
780	50	2.25	10

The information in Table 2 produces an average ice thickness of 156 ±36 cm for the station. This is computed by applying the values in Table 2 directly to eq 31 and 32. The uncertainties are selected from eq 37−40. Given the magnitude of the uncertainties, the results are shown to two significant figures.

Next, consider the spatial and temporal averaging of multiple stations from different cruises in the same region over different times. One does this by first computing the average thickness and uncertainty at a series of stations using the method just applied above. This produces tables (Tables 3−5) that contain positions, time, mean thickness values, and associated uncertainties.

The ship-based averages and uncertainties are computed by taking the station data in Tables 3−5, averaging the mean thickness from each station, and using eq 43 to propagate the uncertainty. This step is particularly important when comparing ship-based observations with the NIC charts, as NIC charts cover a region through which several ship observations may coincide. As an academic exercise and for simplicity, one can further consider climatology based solely on these three cruises. First, one makes an interannual comparison by averaging over the 1995 data (46±4 cm) and comparing them to the average (43±3 cm) from the 1998 data*. The details of the 1995 computation are ($K = 2$) $36 \times 24 / 44 + 59 \times 20 / 44 = 46$ cm and $4 \times 24 / 44 + 5 \times 20 / 44 = 4$ cm.

Conversely, one can compare spring and summer results from the 1990s by looking at the April results in 1995 versus the August results in 1995 and 1998. In this case, the mean thickness and uncertainty in Table 3 are for the former, with the latter equal to 49±4 cm. No scientific interpretation is offered for these answers because this is meant as a computational exercise. A real analysis must include more data than this.

The sequential example shown above works under the assumption that the mean thickness at each station is the estimate the investigator wishes to present as a regional average for a zeroth order estimate for climatological purposes. However, the more comprehensive solution is to propagate the thickness distribution from the station level through to a spatial and temporal distribution. That exercise is left as a challenge to the reader.

---

* With only one cruise in 1998, the results for the 1998 climatology are the same as in Table 5.

Table 3. Tabulated results from Cruise I with a total of 24 stations. The average sea ice thickness is 36±4 cm.

Time				Position		Thickness (cm)	
Day	Month	Year	Hour	Latitude	Longitude	Thickness	Uncertainty
22	4	1995	6	−64.150	111.080	4	22
22	4	1995	8	−64.400	111.100	37	19
22	4	1995	10	−64.667	111.000	39	21
22	4	1995	12	−64.917	111.017	53	22
23	4	1995	0	−65.017	110.783	42	9
23	4	1995	2	−65.200	110.817	47	20
23	4	1995	4	−65.400	110.650	66	32
23	4	1995	6	−65.483	110.200	106	47
24	4	1995	2	−65.767	110.017	37	7
25	4	1995	5	−64.200	111.517	34	19
25	4	1995	7	−64.167	112.067	59	22
25	4	1995	9	−64.183	112.650	52	31
26	4	1995	0	−64.033	116.467	113	42
26	4	1995	2	−64.017	116.967	38	17
26	4	1995	4	−64.000	117.500	42	17
26	4	1995	6	−63.983	118.250	14	6
26	4	1995	8	−64.067	119.117	0	0
26	4	1995	10	−64.300	120.000	0	0
26	4	1995	12	−64.617	120.000	24	5
27	4	1995	0	−64.550	123.900	0	0
27	4	1995	2	−64.633	125.050	2	2
27	4	1995	4	−64.700	125.817	2	2
27	4	1995	6	−64.767	126.567	2	2
27	4	1995	8	−64.883	127.167	0	0

Table 4. Tabulated results from Cruise II with a total of 20 stations. The average sea ice thickness is 59±5 cm.

Time				Position		Thickness (cm)	
Day	Month	Year	Hour	Latitude	Longitude	Thickness	Uncertainty
29	7	1995	23	−61.817	139.850	5	5
30	7	1995	4	−61.950	139.983	38	27
30	7	1995	5	−62.100	139.900	45	21
30	7	1995	6	−62.250	140.000	53	26
30	7	1995	11	−62.433	140.000	36	8
30	7	1995	12	−62.567	139.983	36	8
30	7	1995	13	−62.683	139.933	28	10
30	7	1995	14	−62.783	139.900	22	8
30	7	1995	18	−62.900	139.900	30	7
30	7	1995	19	−63.017	139.933	48	11
30	7	1995	20	−63.167	139.867	52	18
31	7	1995	2	−63.650	139.833	57	23
31	7	1995	4	−63.767	139.867	74	18
31	7	1995	5	−63.833	140.150	0	0
31	7	1995	10	−64.033	140.100	129	30
31	7	1995	11	−64.133	140.050	113	29
31	7	1995	13	−64.283	139.883	138	31
31	7	1995	15	−64.283	140.233	71	14
31	7	1995	17	−64.417	140.333	163	50
31	7	1995	22	−64.550	140.333	47	13

Table 5. Station results from Cruise III with a total of 35 stations. The average sea ice thickness is 43±3 cm.

Time				Position		Thickness (cm)	
Day	Month	Year	Hour	Latitude	Longitude	Thickness	Uncertainty
21	7	1998	11	−63.717	147.183	6	3
21	7	1998	12	−63.867	146.933	55	41
21	7	1998	13	−64.000	146.700	22	7
21	7	1998	14	−64.150	146.483	46	11
21	7	1998	15	−64.283	146.250	44	11
21	7	1998	16	−64.417	146.067	52	13
21	7	1998	17	−64.550	145.867	5	5
21	7	1998	18	−64.667	145.767	0	0
21	7	1998	19	−64.833	145.600	9	6
21	7	1998	20	−64.983	145.450	43	9
21	7	1998	21	−65.117	145.167	91	22
21	7	1998	23	−65.300	145.067	71	15
22	7	1998	2	−65.400	144.867	71	15
25	7	1998	18	−65.133	143.733	167	59
25	7	1998	20	−64.950	143.783	67	22
25	7	1998	21	−64.800	143.817	40	9
25	7	1998	22	−64.667	143.817	82	36
25	7	1998	23	-64.517	143.750	97	47
26	7	1998	0	−64.367	143.717	98	52
26	7	1998	1	−64.233	143.733	42	9
26	7	1998	2	−64.067	143.717	28	6
26	7	1998	3	−63.883	143.700	31	7
26	7	1998	4	−63.767	143.667	25	5
26	7	1998	5	−63.617	143.617	11	4
26	7	1998	6	−63.467	143.550	0	0
26	7	1998	7	−63.317	143.483	0	0
26	7	1998	11	−63.067	143.267	1	1
26	7	1998	12	−62.850	143.250	12	3
26	7	1998	13	−62.700	143.250	0	0

6.2 NIC Example

As stated earlier, the NIC charts (Figure 1) are subjective analysis charts based on a collection of remote sensing imagery, aerial reconnaissance and photography (in the older charts), and subjective annual cycle interpretation (based primarily on the simple degree day model). The recording of these data is based on WMO classification and therefore require some interpretation for value and uncertainty estimates. To resolve this, a set of tables were crafted that include both ASPeCt and NIC classifications in an attempt to quantify thickness with uncertainty from WMO protocols. The current zeroth-order estimate for uncertainty is based on the range provided by the WMO nomenclature, which represents the standard deviation or first sigma of a normal distribution. The results in tabular form are provided in Tables 6 and 7.
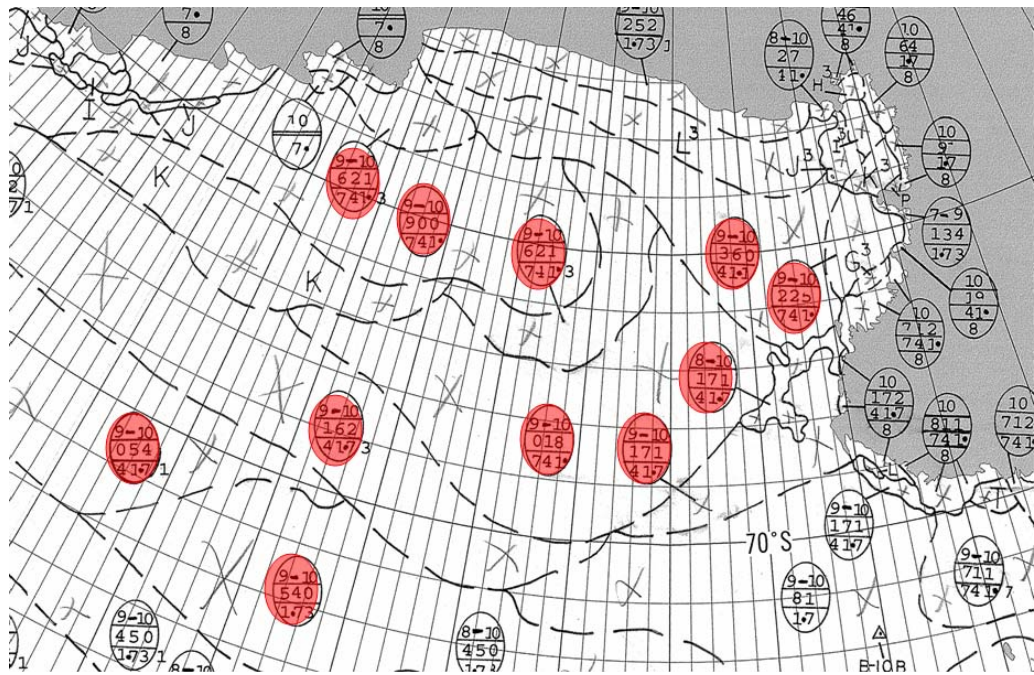

Figure 1. Sample NIC chart of the Ross Sea from 12 September 1997. Egg codes shaded red are the 11 selected samples.

Table 6. Sea ice concentration classification.

Statistical Value		Ship Observation		NIC Classification		
Mean tenth	Range ± tenth	Concentration	ASPeCt Code	Concentration	Egg Code	SIGRID Code
0	0	Open Water	0	Ice Free	00	00
0.5	0.5	–	–	Open Water	0—1	01
–	–	–	–	Bergy	–	02
1	0.5	1/10	1	--	1	10
2	1	–	–	Very Open Water	1—3	13
2	0.5	2/10	2	–	2	20
3	1	–	–	–	2—4	24
3	0.5	3/10	3	–	3	30
4	1	–	–	Very Open to Open	3—5	35
4	0.5	4/10	4	–	4	40
4.5	0.5	–	–	–	4—–5	45
5	1	–	–	Open	4—6	46
5	0.5	5/10	5	–	5	50
6	1	–	–	–	5—7	57
6	0.5	6/10	6	–	6	60
7	1	–	–	Open to Close	6—8	68
7	0.5	7/10	7	–	7	70
8	1	–	–	Close	7—9	79
8	0.5	8/10	8	–	8	80
9	1	–	–	Close to Very Close	8—10	81
9	0.5	9/10	9	–	9	90
9.5	0.5	–	–	Very Close	9—10	91
10	0	10/10	10	Total Concentration	10	92
999	999	No Data	999	No Data	–	99

SIGRID is the sea ice grid notation developed by the NIC for translating hand-drawn charts into a computer formatted system.

Table 7. Sea ice thickness classification.

Statistic		Ship Observation		NIC Chart Classification		
Mean cm	Range± cm	Ice Type	ASPeCt Code	Stage-of-Development	Egg Code	SIGRID Code
0	0	No Ice	0	Ice Free	0	00
5	5	Frazil	10	–	–	–
5	5	Shuga	11	New Ice (<10 cm)	1	81
5	5	Grease	12	–	–	–
5	5	Nilas	20	Nilas (<10 cm)	2	82
10	5	Pancakes	30	–	–	–
12.5	2.5	Young Grey Ice (10–15 cm)	40	Grey Ice (10–15 cm)	4	84
20	10	–	–	Young Ice (10–30 cm)	3	83
22.5	7.5	Young Grey-White Ice (15–30 cm)	50	Grey-White Ice (15–30 cm)	5	85
50	20	First-Year Ice (30–70 cm)	60	White Ice (30–70 cm)	7	87
95	25	First-Year Ice (70–120 cm)	70	First-Year Medium (70–120 cm)	1●	91
115	85	–	–	First-Year Ice (30–200 cm)	6	86
160	40	First-Year Ice (<120 cm)	80	First-Year Thick (<120 cm)	4●	93
160	40	Multiyear Ice	85	Old Ice (>1 year)	7●	95
100	100	Fast Ice	95	Land-Fast Ice	F8	08
999	999	No Data	999	No Data	–	99, -1, 80

The ● symbol is short hand notation for an ice type (e.g., 7● is read as "seven dot" where the number and dot together represent the designated ice type).

Using Figure 2 as a sample, compute an estimate of the sea ice mass of a collection of polygons. In this example, consider the following egg codes and transfer their results into Table 8. Table 9 is used to transcribe the egg code results into representative estimates and associate uncertainties for both concentration and thickness. Finally, in Table 10, the area, thickness, volume, and mass are computed for each polygon.
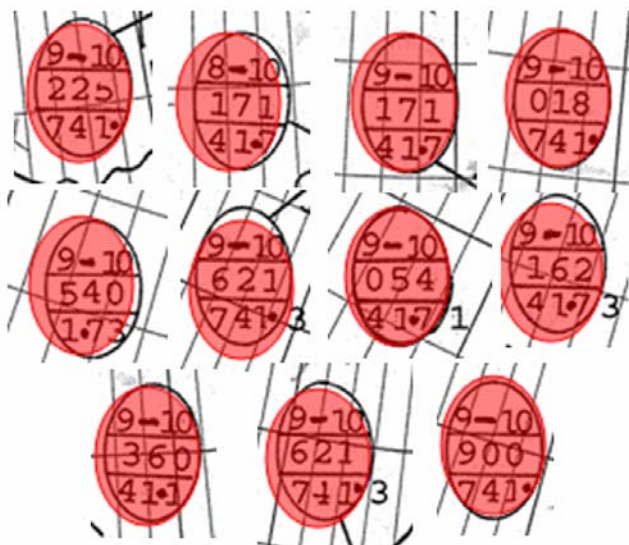
Figure 2. Sample egg codes highlighted in Figure 1. Top line in each egg is the concentration (i.e., Table 6). Middle line numbers represent the concentration for each of the three ice types. Bottom line is the code for the stage-of-development for each of the three ice types.

Table 8. Tabulation of Sample NIC Egg Codes from Figure 2. Concentration is in units of tenths and stage of development is a numeric code as per Table 7.

Concentration				Stage of Development		
Total	Partial 1	Partial 2	Partial 3	Partial 1	Partial 2	Partial 3
9-10	2	2	5	7	4	1•
8-10	1	7	1	4	1•	7
9-10	1	7	1	4	1•	7
9-10	0	1	8	7	4	1•
9-10	5	4	0	1•	7	3
9-10	6	2	1	7	4	1•
9-10	0	5	4	4	1•	7
9-10	1	6	2	4	1•	7
9-10	3	6	0	4	1•	1
9-10	6	2	1	7	4	1•
9-10	9	0	0	7	4	1•

Table 9. Conversion of Sample NIC Egg Codes. Values from Table 8 converted to concentration in tenths and thickness in centimeters with associated uncertainties provided in parenthesis. Conversion computed using Tables 6 and 7. Partial concentrations equal to zero in egg code denotes a trace amount which one assigns an uncertainty of 0.5 tenths.

Concentration				Thickness		
Total	Partial 1	Partial 2	Partial 3	Partial 1	Partial 2	Partial 3
9.5 (0.5)	2 (0.5)	2 (0.5)	5 (0.5)	50 (20)	12.5 (2.5)	95 (25)
9 (1)	1 (0.5)	7 (0.5)	1 (0.5)	12.5 (2.5)	95 (25)	50 (20)
9.5 (0.5)	1 (0.5)	7 (0.5)	1 (0.5)	12.5 (2.5)	95 (25)	50 (20)
9.5 (0.5)	0 (0.5)	1 (0.5)	8 (0.5)	50 (20)	12.5 (2.5)	95 (25)
9.5 (0.5)	5 (0.5)	4 (0.5)	0 (0.5)	95 (25)	50 (20)	20 (10)
9.5 (0.5)	6 (0.5)	2 (0.5)	1 (0.5)	50 (20)	12.5 (2.5)	95 (25)
9.5 (0.5)	0 (0.5)	5 (0.5)	4 (0.5)	12.5 (2.5)	95 (25)	50 (20)
9.5 (0.5)	1 (0.5)	6 (0.5)	2 (0.5)	12.5 (2.5)	95 (25)	50 (20)
9.5 (0.5)	3 (0.5)	6 (0.5)	0 (0.5)	12.5 (2.5)	95 (25)	5 (5)
9.5 (0.5)	6 (0.5)	2 (0.5)	1 (0.5)	50 (20)	12.5 (2.5)	95 (25)
9.5 (0.5)	9 (0.5)	0 (0.5)	0 (0.5)	50 (20)	12.5 (2.5)	95 (25)

Table 10. Estimate of sea ice mass balance for selected polygons. Propagated relative uncertainties of the value are provided in parenthesis. Areas and associated relative uncertainty are determined using ArcInfo on the GIS electronic version of the NIC charts given the position uncertainty of ±10 km for polygon lines as cited in Enomoto and Ohmura (1990).

Area (km^2)	Thickness (cm)	Volume (km^3)	Mass (10^4 kg)
20687 (31%)	60 (24%)	1241 (39%)	1.1 (39%)
12759 (82%)	73 (25%)	928 (85%)	0.8 (85%)
54219 (29%)	73 (25%)	3944 (38%)	3.6 (38%)
253423 (11%)	80 (26%)	20211 (28%)	18.4 (28%)
580007 (12%)	69 (23%)	39730 (26%)	36.2 (26%)
24823 (32%)	42 (32%)	1043 (45%)	0.9 (45%)
299121 (11%)	68 (23%)	20378 (26%)	18.5 (26%)
303500 (13%)	68 (24%)	20714 (27%)	18.8 (27%)
121852 (19%)	61 (26%)	7433 (32%)	6.8 (32%)
61571 (25%)	42 (32%)	2586 (41%)	2.4 (41%)
202702 (11%)	50 (37%)	10211 (39%)	9.3 (39%)

The total area of the polygons in Table 10 is 1,934,664 km² with a relative uncertainty of 5%. Notice how this uncertainty is substantially less than the relative uncertainties of the individual areas listed above. This arises from the summing of uncertainty in quadrature (in other words the variance drops as you get more samples by a rate of $1/N^2$) and is at the heart of the validity of statistics and the necessity of taking multiple samples. The same is true for the mean thickness, which is weighted by the area to a value of 66 cm with relative uncertainty of 12%. The total volume and mass are respectively, 1,284 km³ (12%) and 116×10⁴ kg (12%) with relative uncertainty in parenthesis.

7   CONCLUDING REMARKS

The above mathematical descriptions are the first step in an effort to de-
velop a synthesized data archive of sea ice mass balance. Uncertainties of
each data type must be known (or at least systematically bounded) before
combining with other data. Current uncertainties are based on field obser-
vation estimates and WMO protocols as a first-order estimate. The inten-
tion is to use the current uncertainty estimates as initial testing values but
to refine (and document) new estimates as analysis methods develop. This
type of "meta data" is an important tracking mechanism to determine the
impact of each data type on mass balance calculations. Results demon-
strating the effectiveness of this approach, to date, include Schellenberg
(2002), DeLiberty et al. (2003, 2004), Schellenberg et al. (2002), and Worby
et al. (2002, 2005).

8   REFERENCES

Allison, I., 1989. The East Antarctic sea ice zone: Ice characteristics and drift. *Geojournal,* 18: 103–115.

Allison, I., and A. P. Worby. 1994. Seasonal changes of sea ice characteristics off East Antarctica. *Ann. Glaciol.,* 20*:* 195–201.

Bertoia C., J. Falkingham, and F. Fetterer. 1998. *Polar SAR Data for Operational Sea Ice Mapping, Recent Advances in the Analysis of SAR Data of the Polar Oceans* (R. Kwok and C. Tsatsoulis, Eds.). Berlin: Springer Verlag, p. 201–234.

Dedrick, K. R., K. Partington, M. Van Woert, C. A. Bertoia, and D. Benner. 2001. U. S. National/Naval Ice Center digital sea ice data and climatology. *Canadian Journal of Remote Sensing*, 27(5): 457–475.

DeLiberty, T. L., C. A. Geiger, and M. D. Lemcke. 2004. Examining Sea Ice in the Southern Ocean Using ArcGIS. *Proceedings of the 2004 ESRI International User Conference, 9–13 August, 2004, San Diego, CA*. CD-ROM and website access soon at http://www.esri.com/uc

DeLiberty, T. L., B. A. Schellenberg, C. A. Geiger, A. P. Worby, and M. Van Woert. 2003. Sea ice thickness in the Ross Sea. Illustrated paper, *American Associate of Geographers Meeting, 5–9 March*.

Enomoto, H. and A. Ohmura. 1990. The influences of atmospheric half-yearly cycle on the sea ice extent in the Antarctic. *J. Geophys. Res.*, 95*:* 9497–9511.

Kish, L., 1965. *Survey Sampling*. New York: John Wiley and Sons.

Hines, W. W. and D. C. Montgomery. 1990. *Probability and Statistics in Engineering and Management Science*, 3rd Edition. New York: John Wiley and Sons.

Schellenberg, B. A. 2002. Investigation of sea ice thickness variability in the Ross Sea. M.S. Thesis, University of Delaware.

Schellenberg, B. A., T. L. DeLiberty, C. A. Geiger, J. Silberman, and A. P. Worby. 2002. Investigation of seasonal sea ice thickness variability in the Ross Sea. *Proceedings of 13th Symposium on Global and Climate Variations, American Meteorological Society, Orlando, Florida, 13–17 January*, p. 130–132.

Stark, P. B. 2002. *Statistics Tools for Internet and Classroom Instruction with a Graphical User Interface*. Atomic Dog Publishing. (http://www.stat.berkeley.edu/users/stark/SticiGui/Text/)

Strass, V. H. and E. Fahrbach. 1998. Temporal and regional variation in sea ice draft and coverage in the Weddell Sea obtained from upward looking sonars. In *Antarctic Sea Ice: Physical Processes, Interactions and Variability* (M. O. Jeffries. Ed.). Antarctic Res Ser., 74, p. 12–129.

Thorndike, A. S., D. A. Rothrock, G. A. Maykut, and R. Colony. 1975. The thickness distribution of sea ice. *J. Geophys. Res.,* 80(33): 4501–4513.

Wadhams., P. 1996. Arctic sea ice extent and thickness. In *The Arctic and Environmental Change* (P. Wadhams, J. A. Dowdeswell, and A. N. Schofield, Eds.). Gordon and Breach Publishers, p. 101–119.

Wadhams. P., and J. C. Comiso. 1992. The ice thickness distribution inferred using remote sensing techniques. In *Microwave Remote Sensing of Sea Ice* (F. Carsey, Ed.). Washington: American Geophysical Union, Geophysical Monograph 68, p.375–383.

Worby, A. P., M. O. Jeffries, W. F. Weeks, K. Morris, and R. Jana. 1996. The thickness distribution of sea ice and snow cover during late winter in the Bellingshausen and Amundsen Seas, Antarctica. *J. Geophys. Res.*, 101: 28,441–28,455.

Worby, A. P., R. A. Massom, I. Allison, V. I. Lytle and P. Heil. 1998. East Antarctic sea ice: A review of its structure, properties and drift. In *Antarctic Sea Ice: Physical Processes, Interactions and Variability* (M. O. Jeffries. Ed.). Antarctic Research Series 74, p. 41–67.

Worby, A. P. and S. F. Ackley. 2000. Antarctic research yields circumpolar sea ice thickness data. *EOS Trans, AGU,* 81(17): 181,184–185.

Worby, A. P., C. A. Geiger, T. L. DeLiberty and B. A. Schellenberg. 2002. Circumpolar sea ice thickness maps for the Antarctic. *International Association for Hydraulic Engineering and Research 16th International Symposium on Ice, Dunedin, New Zealand, 2–6 December*.

Worby, A. P., C. A. Geiger, M. Van Woert, S. F. Ackley, and T. D. DeLiberty. 2005. Gamma function parameterization of sea ice thickness distribution. Poster Paper, *Eos Trans. AGU*, 85(47), Fall Meet. Suppl., Abstract and Poster C41C-0216.

World Meteorological Organization (WMO). 1970. *WMO Sea-ice Nomenclature*. Volume 1, *Terminology and Codes*. Report 259. Geneva, Switzerland: World Meteorological Organization.

REPORT DOCUMENTATION PAGE

Public reporting burden for this collection of information is estimated to average 1 hour per response, including the time for reviewing instructions, searching existing data sources, gathering and maintaining the data needed, and completing and reviewing this collection of information. Send comments regarding this burden estimate or any other aspect of this collection of information, including suggestions for reducing this burden to Department of Defense, Washington Headquarters Services, Directorate for Information Operations and Reports (0704-0188), 1215 Jefferson Davis Highway, Suite 1204, Arlington, VA 22202-4302. Respondents should be aware that notwithstanding any other provision of law, no person shall be subject to any penalty for failing to comply with a collection of information if it does not display a currently valid OMB control number. **PLEASE DO NOT RETURN YOUR FORM TO THE ABOVE ADDRESS.**

1. REPORT DATE (DD-MM-YYYY) September 2006	2. REPORT TYPE	3. DATES COVERED (From - To)

4. TITLE AND SUBTITLE

Propagation of Uncertainties in Sea Ice Thickness Calculations from Basin-Scale Operational Observations: A Report Prepared for the International Ice Charting Working Group and the National/Naval Ice Center

5a. CONTRACT NUMBER

5b. GRANT NUMBER
NSF OPP-9818645

5c. PROGRAM ELEMENT NUMBER

6. AUTHOR(S)

Cathleen A. Geiger

5d. PROJECT NUMBER

5e. TASK NUMBER

5f. WORK UNIT NUMBER

7. PERFORMING ORGANIZATION NAME(S) AND ADDRESS(ES)

Cold Regions Research and Engineering Laboratory
U.S. Army Engineer Research and Development Center
72 Lyme Road
Hanover, NH 03755

8. PERFORMING ORGANIZATION REPORT NUMBER

ERDC/CRREL TR-06-16

9. SPONSORING / MONITORING AGENCY NAME(S) AND ADDRESS(ES)

National Science Foundation
Washington, DC

10. SPONSOR/MONITOR'S ACRONYM(S)

11. SPONSOR/MONITOR'S REPORT NUMBER(S)

12. DISTRIBUTION / AVAILABILITY STATEMENT

Approved for public release; distribution is unlimited

13. SUPPLEMENTARY NOTES

14. ABSTRACT

Sea ice serves as a natural flux monitor of the global heat balance. This capability is attributed to the unique location of sea ice at the interface of the world's two largest circulation systems—the air and ocean. The increased awareness of warming in the polar region has precipitated increased efforts to measure sea ice thickness as an index for global heat changes. This increased awareness has brought with it the development of several new prototype in situ, telemetry, and satellite remote sensing instruments. Each of these provides a means for measuring part or all of the frozen material at the air–sea interface, but each comes with considerable limitations. The integration of these measurements into basin-scale objective analysis fields will serve as important input for global climate models, much like current-day weather forecasting systems and the Toga-Toa El-Niño monitoring system. As the various thickness monitoring tools begin to develop, it is critical that standards be established to record the quality of these data. This report addresses the data quality issues by examining a robust method for tracking uncertainties in measurements. The data sets considered are the two existing operational basin-scale systems: ship-based observations and satellite composite analysis. Illustrative examples are included.

15. SUBJECT TERMS

Climate change
Data analysis
Data collection
Global heat balance
Sea ice

16. SECURITY CLASSIFICATION OF:			17. LIMITATION OF ABSTRACT	18. NUMBER OF PAGES	19a. NAME OF RESPONSIBLE PERSON
a. REPORT	**b. ABSTRACT**	**c. THIS PAGE**	U	41	**19b. TELEPHONE NUMBER** (include area code)
U	U	U			